Available online at www.sciencedirect.com
SCIENCE DIRECT
Physics Letters A 353 (2006) 273–280
PHYSICS LETTERS A
www.elsevier.com/locate/pla

Nonlinear acoustic propagation in homentropic perfect gases: A numerical study

Ivan Christov [a,1], P.M. Jordan [a,*], C.I. Christov [b]

[a] *Code 7181, Naval Research Laboratory, Stennis Space Center, MS 39529, USA*
[b] *Department of Mathematics, University of Louisiana at Lafayette, Lafayette, LA 70504, USA*

Received 28 December 2005; accepted 29 December 2005

Available online 9 January 2006

Communicated by R. Wu

Abstract

A study of nonlinear acoustic waves in a homentropic perfect gas is presented. Conservation laws for the Euler and Lighthill–Westervelt equations are constructed and solved numerically using a Godunov-type finite-difference scheme. Simulations are carried out in the context of two initial-boundary-value problems (IBVP)s—one resulting in finite-time, and the other in infinite-time, blow-up at the wavefront. Additionally, analytical results are presented to support the numerical findings.

PACS: 43.25.+y; 47.40.-x; 31.15.Fx

Keywords: Godunov-type MUSCL scheme; Lighthill–Westervelt equation; Euler equations; Shock formation; Acceleration waves

1. Introduction

The study of nonlinear acceleration waves, which is a branch of singular surface theory, has been, and remains, an area of considerable interest in continuum mechanics [1]. The feature that these waves are best known for, and that which distinguishes such propagating wavefronts from other nonlinear waves such as solitons, is the phenomenon of *finite-time blow-up* (or gradient catastrophe), whereby the wave's amplitude develops a singularity at a particular (finite) time. In 1967, Coleman and Gurtin [2] conjectured that finite-time blow-up implied that a shock wave had, in fact, formed. They noted, however, that a rigorous proof of their supposition was lacking. Over the years, many examples of this phenomenon have been documented in the literature of continuum mechanics (see, e.g., Refs. [1–9] and those therein).

The numerical study of shocks (especially in fluid dynamics) has been a subject of considerable interest since the 1950s (see, e.g., Chapter 5 of Ref. [10]). However, the hyperbolic equations that govern such phenomena, e.g., the blow-up of acceleration waves, are difficult to solve numerically. The numerical solutions produced by standard finite-difference methods usually lose monotonicity, due to the generation of spurious oscillations in regions of large gradients (i.e., front steepening). As noted by Jordan and Christov [7], a second-order accurate version of their simple finite-difference scheme is not readily available. In practice, one rarely finds suitable (i.e., monotone) standard finite-difference schemes with a high order of accuracy. The reason for this can be traced back to a theorem by Godunov, which states that monotone schemes of order two (or higher) do not exist for the linear advection equation (see, e.g., Ref. [10] and those therein). Godunov's work in the 1950s [11] prompted the development of a wide array of shock-capturing numerical algorithms. In particular, van Leer's seminal series of papers in the 1970s, culminating with [12], led to the development of higher-order-accurate extensions of Godunov's method. Books such as Toro's [10] and LeVeque's [13] discuss a large number of these advances. To date, the most successful shock-capturing

* Corresponding author. Tel.: +1 228 688 4338; fax: +1 228 688 5049.
E-mail address: pjordan@nrlssc.navy.mil (P.M. Jordan).
[1] Present address: Department of Mathematics, Texas A&M University, College Station, TX 77843, USA.

0375-9601/$ – see front matter
doi:10.1016/j.physleta.2005.12.101

numerical methods are those developed for systems of hyperbolic conservation laws.

Our intent here is to carry out an in-depth, numerical study of acceleration wave blow-up in homentropic perfect gases using a Godunov-type (i.e., shock-capturing and conservative) numerical schemes. We consider both the Euler equations and the Lighthill–Westervelt (LW) equation, the latter stemming from imposing the finite-amplitude approximation in conjunction with the linear-impedance assumption on the former. We compare and contrast the LW model with the Euler equations in the context of two IBVPs that involve the input of a sinusoidal, signal-type boundary condition. To this end, the present Letter is arranged as follows. In Section 2, the exact Euler equations for a perfect gas are reduced to a single equation for the acoustic potential. In Section 3, an acceleration wave analysis of the 1D Euler equations is presented, and the break-down time is determined. In Section 4, we derive the LW equation from the exact 1D potential equation, and we show that the former is equivalent to a first-order system of nonlinear equations. In Section 5, we discuss the Godunov-type finite-difference scheme that we use for our simulations. In Section 6, we formulate both systems of equations (i.e., LW and Euler) as conservation laws and present the numerical solutions to the two IBVPs. Lastly, in Section 6 results are compared and in Section 7 conclusions are stated.

2. Balance laws, equation of state, and basic assumptions

Consider a lossless, compressible fluid, which we assume behaves as a perfect gas, that is initially in its equilibrium state. The equations of continuity, momentum, energy, and state governing the homentropic flow of such a gas, referred to collectively as the Euler equations, are

$$\dot{\varrho} + \varrho \nabla \cdot \mathbf{v} = 0, \tag{1}$$

$$\mathbf{v}_t + \frac{1}{2}\nabla|\mathbf{v}|^2 - \mathbf{v} \times (\nabla \times \mathbf{v}) = -\varrho^{-1}\nabla\wp, \tag{2}$$

$$\dot{\eta} = 0, \tag{3}$$

$$\wp = \wp_0(\varrho/\varrho_0)^\gamma, \tag{4}$$

where $\mathbf{v}$ is the velocity vector, ϱ (> 0) is the mass density, $\wp$ is the thermodynamic pressure, η is the specific entropy, the constant γ (> 1) denotes the ratio of specific heats [14], all body forces have been neglected, and a superposed dot denotes the material derivative. Furthermore, Eq. (3) is a consequence of the homentropic assumption[2] $\eta = \text{const}$, where in the present Letter this constant is the equilibrium value η_0. And by equilibrium state we mean the unperturbed, quiescent state in which, along with $\eta = \eta_0$, $\varrho = \varrho_0$, $\wp = \wp_0$, and $\mathbf{v} = \mathbf{0}$, where ϱ_0 and $\wp_0$ are positive constants.

Since the flow is assumed homentropic, it follows that $\varrho^{-1}\nabla\wp = \nabla h$, where h is the specific enthalpy [14]. Making this substitution, and then taking the curl of Eq. (2), it can be shown that $\nabla \times \mathbf{v} = 0$, for all $t \geqslant 0$, since the flow was initially irrotational [14]. Consequently, $\mathbf{v} = \nabla\phi$, where ϕ is the scalar velocity (or acoustic) potential, and Eq. (2) reduces to

$$\nabla\phi_t + \frac{1}{2}\nabla|\nabla\phi|^2 + \nabla h = 0. \tag{5}$$

Next, we introduce the following thermodynamic relations, all of which are easily established using the definition of h and the perfect gas law [15]:

$$\nabla h = (\gamma-1)^{-1}\nabla c^2, \qquad \varrho_t = 2\varrho c_t\big\{c(\gamma-1)\big\}^{-1},$$
$$\nabla\varrho = c^{-2}\nabla\wp, \tag{6}$$

where $c = \sqrt{\gamma\wp/\varrho}$ denotes the sound speed in the disturbed gas.

Using these relations, we recast Eqs. (1) and (5) as (see, e.g., [16])

$$\big\{\partial_t + (\nabla\phi)\cdot\nabla\big\}c^2 + (\gamma-1)c^2\nabla^2\phi = 0, \tag{7}$$

$$c^2 = c_0^2 - (\gamma-1)\left\{\phi_t + \frac{1}{2}|\nabla\phi|^2\right\}, \tag{8}$$

where the constant $c_0 = \sqrt{\gamma\wp_0/\varrho_0}$ denotes the sound speed in the undisturbed gas. Using Eq. (8), c^2 can be eliminated from Eq. (7) to yield, after some simplification,

$$c_0^2\nabla^2\phi - \phi_{tt} - \partial_t|\nabla\phi|^2 - \frac{1}{2}(\nabla\phi)\cdot\nabla|\nabla\phi|^2 - (\gamma-1)\left\{\phi_t + \frac{1}{2}|\nabla\phi|^2\right\}\nabla^2\phi = 0. \tag{9}$$

This PDE, which has been derived in a number of works (see, e.g., Refs. [16–18]), describes the homentropic flow of a perfect gas in terms of the acoustic potential ϕ. In the one-dimensional (1D) case, assuming propagation along the x-axis, Eq. (9) reduces to (see also [19])

$$c_0^2\phi_{xx} - \phi_{tt} - 2\phi_x\phi_{tx} - (\gamma-1)\phi_t\phi_{xx} - \frac{1}{2}(\gamma+1)(\phi_x)^2\phi_{xx} = 0, \tag{10}$$

where $\mathbf{v} = (\phi_x, 0, 0) = (u(x,t), 0, 0)$.

3. Acceleration wave analysis

Returning to the set of Euler equations but now limiting our attention to 1D propagation along the x-axis, we can recast Eqs. (1) and (2) as

$$\varrho_t + u\varrho_x + \varrho u_x = 0,$$
$$\varrho(u_t + uu_x) = -\wp_\varrho\varrho_x, \tag{11}$$

where $\dot{\eta} = 0$ still holds, and from Eq. (4) we find that

$$\wp_\varrho = c_0^2(\varrho/\varrho_0)^{\gamma-1}. \tag{12}$$

Consider now a smooth planar surface $x = \Sigma(t)$ propagating to the right along the x-axis of a Cartesian coordinate system into a region $\mathcal{R}$ filled with a perfect gas in its equilibrium state. Suppose that $u, \varrho \in C(\mathcal{D}_1)$, where $\mathcal{D}_1 = \{(x,t)\colon\ x \in \mathcal{R}, t \in \mathbb{R}^+\}$, and $u, \varrho \in C^2(\mathcal{D}_2)$, where $\mathcal{D}_2 = \{(x,t)\colon\ x \in (\mathcal{R}\setminus\Sigma), t \in \mathbb{R}^+\}$, but that at least one of the first derivatives of u or ϱ, say

[2] That is, $\dot{\eta} = 0$ and $\nabla\eta = 0$; see [14].

u_t, can suffer a jump discontinuity (or jump) on crossing Σ; i.e., $[u] = [\varrho] = 0$ but $[u_t]$ can be nonzero. Here, $[\mathfrak{F}]$ denotes the amplitude of a jump in the function $\mathfrak{F} = \mathfrak{F}(x,t)$ across Σ and is defined by

$$[\mathfrak{F}] \equiv \mathfrak{F}^- - \mathfrak{F}^+, \tag{13}$$

where $\mathfrak{F}^\mp \equiv \lim_{x\to\Sigma(t)^\mp} \mathfrak{F}(x,t)$ are assumed to exist and a '+' superscript corresponds to the region into which Σ is advancing while a '−' superscript corresponds to the region behind Σ. If $[u_t] \neq 0$, then the surface Σ is termed an acceleration wave [1]. Hence, given the above, and assuming that the value of $[u_t]$ is known at $t = 0$, we set ourselves the task of determining the behavior of $[u_t]$ for all $t > 0$.

The first step in the process is employing Hadamard's lemma [1,2]:

$$\frac{\mathfrak{D}[\mathfrak{F}]}{\mathfrak{D}t} = [\mathfrak{F}_t] + V[\mathfrak{F}_x], \tag{14}$$

where $\mathfrak{D}/\mathfrak{D}t$ is the (one-dimensional) displacement derivative[3] and $|V|(\neq 0)$ is the speed of Σ with respect to the gas immediately ahead. Then, invoking the assumptions $[u] = [\varrho] = 0$, along with Eq. (14), we obtain the jump relations

$$V[u_x] + [u_t] = 0, \qquad V[\varrho_x] + [\varrho_t] = 0. \tag{15}$$

Next, we take the jumps of Eqs. (11), which is permissible since they hold on both sides of Σ. This yields, after employing the formula for the jump of a product,

$$[\mathfrak{F}\mathfrak{G}] = \mathfrak{F}^+[\mathfrak{G}] + \mathfrak{G}^+[\mathfrak{F}] + [\mathfrak{F}][\mathfrak{G}], \tag{16}$$

the two additional jump equations

$$[\varrho_t] + \varrho_0[u_x] = 0, \qquad \varrho_0[u_t] + c_0^2[\varrho_x] = 0, \tag{17}$$

where we note that $u^+ = 0$, $\varrho^+ = \varrho_0$, and $\wp_\varrho^+ = c_0^2$ since the gas ahead of Σ is in its equilibrium state. Our next step is to determine V. For this, we set the determinant of the coefficient matrix of this system of (four) jump equations to zero. This leads to the equation $V^2 = c_0^2 (= \wp_\varrho^+)$, and consequently the solution $V = c_0$, where the negative solution has been discarded since we have taken Σ to be right-traveling. Additionally, we note the following relations:

$$[u_x] = -c_0^{-1}A, \qquad [\varrho_t] = \varrho_0 c_0^{-1}A, \qquad [\varrho_x] = -\varrho_0 c_0^{-2}A, \tag{18}$$

where $A(t) \equiv [u_t]$, which are derived directly from Eqs. (15) and (17).

Although we omit the remaining details, it is a relatively straightforward process using Hadamard's lemma, Eqs. (11), and the above jump relations, to derive the nonlinear, ordinary differential equation

$$\frac{\mathfrak{D}A}{\mathfrak{D}t} - \left(\frac{\gamma+1}{2c_0}\right)A^2 = 0. \tag{19}$$

[3] That is, the time-rate-of-change measured by an observer traveling with Σ.

Eq. (19) is of the Bernoulli type; its exact solution, which has been exhaustively studied, is

$$A(t) = \frac{A(0)}{1 - \{c_0^{-1}A(0)(\gamma+1)/2\}t}, \tag{20}$$

where $A(0)$ denotes the value of $[u_t]$ at time $t = 0$.

According to Eq. (20), the evolution of $A(t)$ can qualitatively be described as follows:

(i) If $A(0) < 0$, then $A(t) \to 0$ from below as $t \to \infty$.
(ii) If $A(0) = 0$, then $A(t) = 0$ for all $t \geqslant 0$.
(iii) If $A(0) > 0$, then $\lim_{t\to t_\infty} A(t) = \infty$, where the breakdown time is

$$t_\infty = \frac{2c_0}{A(0)(\gamma+1)}. \tag{21}$$

Finally, we observe that, in the case of a perfect gas, the expressions for Σ's speed and amplitude given here based on the Euler equations are *identical* to their LW counterparts given in Ref. [7].

4. The Lighthill–Westervelt equation

In this section, we present a derivation of a simpler 1D equation for the acoustic potential by applying the finite-amplitude approximation to Eq. (10). To this end, we begin by introducing the following nondimensional variables:

$$\phi' = \phi/(UL), \qquad x' = x/L, \qquad t' = t(c_0/L),$$
$$u' = u/U, \qquad \varrho' = \varrho/\varrho_0, \tag{22}$$

where U (> 0) and L (> 0) denote a characteristic speed and length, respectively, and we note that Eqs. $(22)_4$ and $(22)_5$ will not be needed until end of this section. Consequently, Eq. (10) is recast in dimensionless form as

$$\begin{aligned}&\big[1 - \epsilon(\gamma-1)\phi_t\big]\phi_{xx} - 2\epsilon\phi_x\phi_{tx} - \phi_{tt}\\ &\quad = \frac{1}{2}\epsilon^2(\gamma+1)(\phi_x)^2\phi_{xx},\end{aligned} \tag{23}$$

where $\epsilon \equiv U/c_0$ is the Mach number and all primes have been omitted but are understood. Multiplying both sides by $[1 - \epsilon(\gamma-1)\phi_t]^{-1}$ and then expanding in a binomial series, assuming that $0 < \epsilon \ll 1$ is sufficiently small, yields

$$\begin{aligned}&\phi_{xx} - 2\epsilon\big[1 + \epsilon(\gamma-1)\phi_t + \mathcal{O}\big(\epsilon^2\big)\big]\phi_x\phi_{tx}\\ &\quad - \big[1 + \epsilon(\gamma-1)\phi_t + \mathcal{O}\big(\epsilon^2\big)\big]\phi_{tt}\\ &\qquad = \frac{1}{2}\epsilon^2(\gamma+1)\big[1 + \epsilon(\gamma-1)\phi_t + \mathcal{O}\big(\epsilon^2\big)\big](\phi_x)^2\phi_{xx}.\end{aligned} \tag{24}$$

If terms of order $\mathcal{O}(\epsilon^2)$ are now neglected, then, after simplifying, we obtain

$$\phi_{xx} - \phi_{tt} = \epsilon\left\{(\phi_x)^2 + \frac{1}{2}(\gamma-1)(\phi_t)^2\right\}_t, \tag{25}$$

which is the lossless version of Kuznetsov's equation [15].

The final step in the derivation, which is not part of the finite-amplitude approximation, is to assume propagation to the

right and employ the linear-impedance relation $\phi_x \approx -\phi_t$ (see, e.g., [18]) only on the right-hand (i.e., the perturbing) side of Eq. (25). Making this replacement and rearranging terms, we arrive at the (dimensionless) LW equation for a perfect gas, namely,

$$\phi_{xx} - \left[1 + \epsilon(\gamma+1)\phi_t\right]\phi_{tt} = 0. \tag{26}$$

As shown in [7], the (1D) LW equation can be expressed as a first-order system. To rederive this system in terms of the nondimensional quantities given in Eq. (22), we make use of the fact that $u \equiv \phi_x$ and that the nondimensional acoustic density $\rho \equiv \varrho - 1$, which is also known as the condensation, is related to the potential via $\rho = -\epsilon\phi_t$. Hence, we have $\phi_t = \epsilon^{-1}(1-\varrho)$ and, assuming that $\phi_{xt} = \phi_{tx}$ holds, we also have $u_t = -\epsilon^{-1}\varrho_x$. Thus, it follows that Eq. (26) can be recast as the system

$$\begin{aligned} &u_t + \epsilon^{-1}\varrho_x = 0, \\ &\varrho_t + (1 + 2\beta - 2\beta\varrho)^{-1}\epsilon u_x = 0. \end{aligned} \tag{27}$$

Here, we note that in the case of perfect gases, the ratio of specific heats γ is related to the coefficient of nonlinearity β via $\beta = (\gamma+1)/2$. Note that this system is *not* in the form of a conservation law. In fact, neither is the system consisting of Eqs. (1)–(4). Thus, the Godunov-type scheme, which we discuss in Section 5, cannot be applied to either of these systems in their current forms. However, in Section 6 we show how the latter issue can be resolved.

5. The MUSCL–Hancock scheme

In this section, we describe the high-resolution Godunov-type conservative numerical method that we apply to the Euler and LW equations derived in Sections 2 and 4. In particular, we summarize our implementation of the MUSCL–Hancock scheme (as described in [10]), which is a $\mathcal{O}[(\Delta x)^2 + (\Delta t)^2]$ accurate method, in regions of smooth flow. The latter employs van Leer's monotone upstream scheme for conservation laws (MUSCL) to achieve second-order accuracy in space via a nonlinear reconstruction of cell-interface values; second-order accuracy in time is obtained through predictor-corrector time-stepping.

Hence, let us consider the general hyperbolic conservation law

$$\mathbf{Q}_t + \mathbf{F}(\mathbf{Q})_x = 0, \tag{28}$$

where $\mathbf{Q}$ and $\mathbf{F}(\mathbf{Q})$ are column vectors containing the conserved quantities and their corresponding fluxes, respectively. Moreover, for the case at hand, the conserved quantities are functions of ϱ and u. To this end, given domain $[0, l]$, we construct a N-cell staggered grid, such that the cells' centers are located at $x_i = (i + \frac{1}{2})\Delta x$ where $\Delta x = l/N$ and $0 \leqslant i \leqslant N-1$. Moreover, we use the average of $\mathbf{Q}$ over the ith cell at time $t = t_n$ (i.e., at the nth time step), denoted by $\mathbf{Q}_i^n$, as the value of the conserved quantities at the center of that cell. Consequently, the value of $\mathbf{Q}$ at the left and right interface of the ith cell (again, at time $t = t_n$) is denoted by $\mathbf{Q}^n_{i-\frac{1}{2}}$ and $\mathbf{Q}^n_{i+\frac{1}{2}}$, respectively.

We approximate the conservation law in Eq. (28) via the *conservative* discretization

$$\mathbf{Q}_i^{n+1} = \mathbf{Q}_i^n + \frac{\Delta t}{\Delta x}\left(\mathbf{F}^n_{i-\frac{1}{2}} - \mathbf{F}^n_{i+\frac{1}{2}}\right), \tag{29}$$

where $\mathbf{F}^n_{i-\frac{1}{2}}$ and $\mathbf{F}^n_{i+\frac{1}{2}}$ denote the fluxes through the left and right interface of the ith cell, respectively. Note that Eq. (29) is derived from the integral form of the conservation law, hence it admits weak solutions to Eq. (28) and is shock-capturing [10,13]. Below we discuss how to compute the fluxes at each time step and obtain second-order accuracy in space and time. And henceforth we take the temporal superscript n to be understood.

The discretization given in Eq. (29) is only first-order accurate is space and in time. To obtain second-order accuracy in space we perform a slope-limited, linear reconstruction of the cell-interface values of $\mathbf{Q}$ based upon the cell-center values. In other words, we choose

$$\begin{aligned} \mathbf{Q}_i^{\mathrm{L}} &= \mathbf{Q}_i - \frac{\Phi}{2}(\mathbf{Q}_i - \mathbf{Q}_{i-1}), \\ \mathbf{Q}_i^{\mathrm{R}} &= \mathbf{Q}_i + \frac{\Phi}{2}(\mathbf{Q}_i - \mathbf{Q}_{i-1}), \end{aligned} \tag{30}$$

to be the values of $\mathbf{Q}$ at the ith cell's left and right interface, respectively. In the above equations, Φ represents for the "min-mod" *nonlinear* limiter:

$$\Phi = \max\left[0, \min\left(1, \frac{\mathbf{Q}_{i+1} - \mathbf{Q}_i}{\mathbf{Q}_i - \mathbf{Q}_{i-1}}\right)\right]. \tag{31}$$

The nonlinear limiter is necessary for the scheme to be total variation diminishing (TVD) and thus monotonicity preserving, i.e., no spurious oscillations are introduced in the solution.

Upon extrapolating the cell-interface values of $\mathbf{Q}$, we perform a predictor time step to obtain the *evolved* cell-interface values:

$$\bar{\mathbf{Q}}_i^{\mathrm{L,R}} = \mathbf{Q}_i^{\mathrm{L,R}} + \frac{1}{2}\frac{\Delta t}{\Delta x}\left[\mathbf{F}\left(\mathbf{Q}_i^{\mathrm{L}}\right) - \mathbf{F}\left(\mathbf{Q}_i^{\mathrm{R}}\right)\right]. \tag{32}$$

Then, we set up a *local* Riemann problem (RP) on the right, or *upwind*, interface of ith cell. That is to say, the RP is solved in the local coordinate system with origin $\tilde{x} = 0$, which is located at the global cell-interface $x = x_{i+\frac{1}{2}}$. Moreover, the initial data for the RP is taken to be

$$\mathbf{Q}_0 = \begin{cases} \mathbf{Q}_{\mathrm{L}} \equiv \bar{\mathbf{Q}}_i^{\mathrm{R}}, & \tilde{x} \leqslant 0, \\ \mathbf{Q}_{\mathrm{R}} \equiv \bar{\mathbf{Q}}_{i+1}^{\mathrm{L}}, & \tilde{x} > 0. \end{cases} \tag{33}$$

The solution to the above RP determines the flux through the cell-interface.

In order to decrease the computational time and the complexity of the algorithm, rather than computing the *exact* solution to the RP at each interface, we obtain an *approximate* solution to the RP via the method of Harten, Lax and van Leer (HLL) [10,20]. Moreover, we never need to find the *explicit* solution to the RP because, according to the HLL algorithm, the

intercell flux $\mathbf{F}_{i+\frac{1}{2}}$ can be approximated by

$$\mathbf{F}^{\mathrm{HLL}} = \begin{cases} \mathbf{F}_{\mathrm{L}}, & 0 \leqslant S_{\mathrm{L}}, \\ \frac{S_{\mathrm{R}}\mathbf{F}_{\mathrm{L}} - S_{\mathrm{L}}\mathbf{F}_{\mathrm{R}} + S_{\mathrm{L}}S_{\mathrm{R}}(\mathbf{Q}_{\mathrm{R}} - \mathbf{Q}_{\mathrm{L}})}{S_{\mathrm{R}} - S_{\mathrm{L}}}, & S_{\mathrm{L}} < 0 < S_{\mathrm{R}}, \\ \mathbf{F}_{\mathrm{R}}, & S_{\mathrm{R}} \leqslant 0, \end{cases} \tag{34}$$

where $\mathbf{F}_{\mathrm{L,R}} \equiv \mathbf{F}(\mathbf{Q}_{\mathrm{L,R}})$. Furthermore, S_{L} and S_{R} (by assumption, $S_{\mathrm{L}} \leqslant S_{\mathrm{R}}$) denote the speed of the fastest and slowest moving waves in the solution to the RP, respectively. But, since we do not solve the Riemann problem explicitly, we approximate the wave speeds by

$$S_{\mathrm{L}} = -S_{\mathrm{R}}, \quad S_{\mathrm{R}} = \max\bigl(|u_{\mathrm{L}}| + \mathfrak{c}_{\mathrm{L}}, |u_{\mathrm{R}}| + \mathfrak{c}_{\mathrm{R}}\bigr), \tag{35}$$

where $\mathfrak{c}_{\mathrm{L,R}}$ denote the local sound speed $\mathfrak{c}$ on each side of the interface. Also, we note that under the nondimensionalization scheme given in Eq. (22), the (local) sound speeds in the undisturbed and disturbed gas are one and $\mathfrak{c} \equiv c/c_0 = \sqrt{\varrho^{\gamma-1}}$, respectively. We found the estimates given by Eq. (35) to be robust and to provide good results for various wave states of the RP (see, e.g., [10] for other choices). Furthermore, note that computing the intercell flux via Eq. (34) from the evolved Riemann data in Eq. (33) constitutes a corrector time step, resulting in a scheme that is of second-order accuracy in time.

The stability of any explicit finite-difference method, such as the one described above, is contingent upon the Courant–Friedrichs–Levy (CFL) condition, i.e., the time step must be such that

$$\Delta t \leqslant \frac{\Delta x}{S^n_{\max}} \quad \Leftrightarrow \quad \Delta t = \frac{C_{\mathrm{CFL}}\Delta x}{S^n_{\max}}, \tag{36}$$

where $S^n_{\max}$ denotes the speed of the fastest intercell wave at time $t = t_n$ and C_{CFL} the Courant number ($0 < C_{\mathrm{CFL}} \leqslant 1$). In practice, the C_{CFL} is determined empirically. In addition, we obtain a reliable estimate of the largest intercell wave speed from Eq. (35) (see, e.g., [10] for other choices):

$$S^n_{\max} = \max_{-1 \leqslant i \leqslant N-1} S_{\mathrm{R}}. \tag{37}$$

The physical problems that we solve in Section 6 require the use of both *transmissive* and *reflective* boundary conditions. These boundary conditions are implemented via two *ghost* cells on each end of grid. For the transmissive case we require that

$$\begin{aligned} \varrho_{-1} &= \varrho_0, \qquad u_{-1} = u_0, \\ \varrho_{-2} &= \varrho_1, \qquad u_{-2} = u_1, \end{aligned} \tag{38}$$

where the subscript denotes the cell's index; an index $i > N-1$ or $i < 0$ corresponds to a ghost cell beyond the computational grid. Likewise, for the reflective case we require that

$$\begin{aligned} \varrho_N &= \varrho_{N-1}, \qquad u_N = -u_{N-1}, \\ \varrho_{N+1} &= \varrho_{N-2}, \qquad u_{N+1} = -u_{N-2}. \end{aligned} \tag{39}$$

Note that we must use two, rather than one, ghost cells to be able to perform a second-order-accurate reconstruction of the cell-interface values at the boundaries of the grid.

It is known that the shock-resolution and stability of Godunov-type schemes, which use the MUSCL reconstruction, depend on the choice of limiter. In addition to the minmod limiter, we tested the "superbee" limiter and van Leer's "MC" limiter. We found that, for the IBVPs solved in Section 6, the minmod limiter gives the best results. In order to validate the scheme we conducted calculations with different grid sizes. Using $N = 1000, 2000, 4000, 8000, 16\,000$, we found that (in the regions of smooth flow) the difference between the solution on each grid and the solution on the largest grid decreased quadratically, in the L_1 norm. In the next section, we show the results for $N = 4000$ and $C_{\mathrm{CFL}} = 0.3$.

6. Results and discussion

In order to apply the numerical method described in Section 5 to the systems given in Sections 2 and 4, both must be expressed as conservation laws. For the LW system [Eq. (27)], we introduce the change of variable

$$\begin{aligned} &\tilde{\varrho} = (1+2\beta)\varrho - \beta\varrho^2 \quad \Leftrightarrow \\ &\varrho = \frac{1}{2\beta}\left\{2\beta + 1 \mp \sqrt{(2\beta+1)^2 - 4\beta\tilde{\varrho}}\right\}. \end{aligned} \tag{40}$$

Note that the "$-$" sign must be selected here so that $\varrho \to 0$ only when $\tilde{\varrho} \to 0$. Consequently, by substituting Eq. (40) into Eq. (27), we obtain the conservation law

$$\begin{pmatrix} \tilde{\varrho} \\ u \end{pmatrix}_t + \begin{pmatrix} \epsilon u \\ (2\beta\epsilon)^{-1}\{2\beta + 1 - \sqrt{(2\beta+1)^2 - 4\beta\tilde{\varrho}}\} \end{pmatrix}_x = 0. \tag{41}$$

The 1D Euler equations (11) can be expressed as a conservation law by adding the second equation to the first and then using Eq. (12), the equation of state, to eliminate $\wp$. This yields a system that, in dimensionless form, is given by

$$\begin{pmatrix} \varrho \\ \varrho u \end{pmatrix}_t + \begin{pmatrix} \epsilon\varrho u \\ \epsilon\varrho u^2 + \epsilon^{-1}\varrho^{\gamma}/\gamma \end{pmatrix}_x = 0, \tag{42}$$

where $\epsilon \equiv U/c_0$ is the Mach number as before, and we continue to omit the (understood) primes.

Consider now the two systems given by Eqs. (41) and (42) subject to the following initial and boundary conditions:

$$\begin{aligned} &\rho(x,0) = 0, \qquad u(x,0) = 0, \\ &\rho(0,t) = \bigl[H(t) - H(t-t_w)\bigr] f(t), \end{aligned} \tag{43}$$

where $H(\cdot)$ denotes the Heaviside unit step function, we recall that $\rho \equiv \varrho - 1$ denotes the dimensionless acoustic density, and two forms of the periodic function f will be considered. Note that the first two conditions reflect the fact that the medium ahead of Σ is in its equilibrium state, and the third means that a pulse of finite duration (or width) t_w is introduced at the boundary $x = 0$ at time $t = 0+$. For the simulations below, we use $t_w = 1$.

To compare and contrast the LW and Euler systems, as well as evaluate the performance of our numerical method, we consider two different input signals, or boundary conditions (BC)s, $f(t)$. In the first case, we take $f(t) = \epsilon \sin(\pi t)$. As noted in [7], with this BC the first derivative of $f(t)$ suffers a jump across $t = 0$. Moreover, such an (compressive) input signal will lead

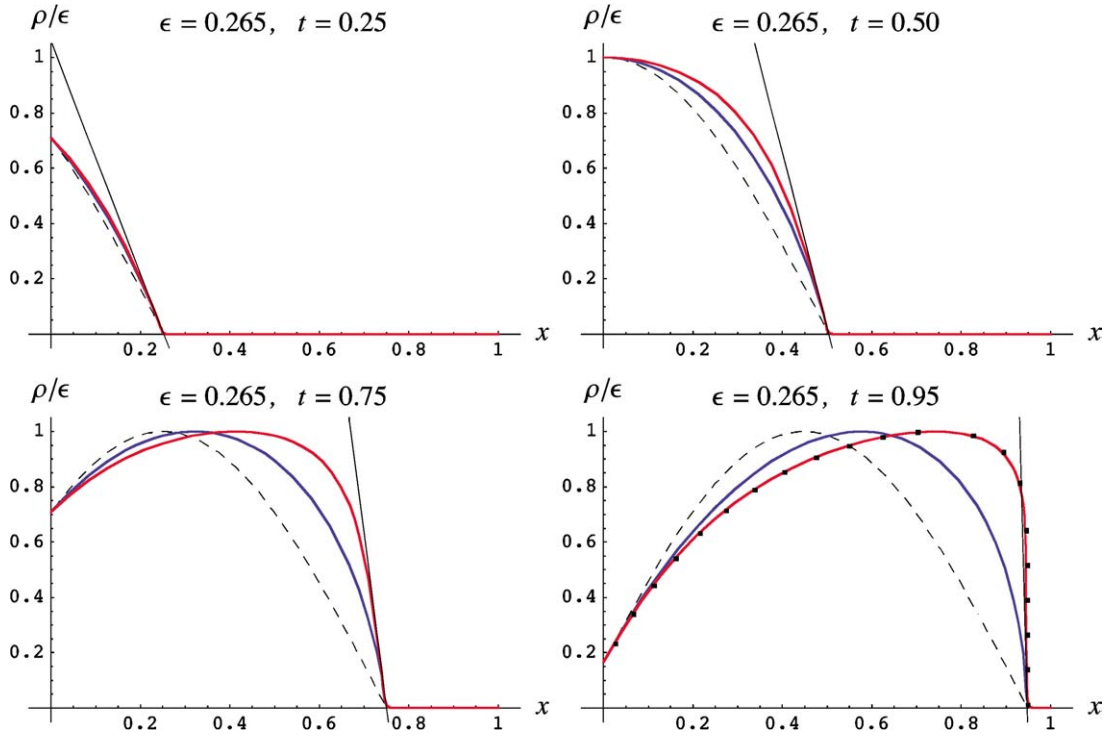

Fig. 1. Four snapshots in time of the scaled dimensionless acoustic density, ρ/ϵ, vs. x for $f(t) = \epsilon \sin(\pi t)$.

to amplitude blow-up in finite time, strongly suggesting the formation of a shock (see Section 3 and Ref. [7]). The second BC considered is $f(t) = \epsilon \sin^2(\pi t)$, where both $f(t)$ and its first derivative $f'(t)$ are continuous across $t = 0$. Hence, there is *no* acceleration wave at the wavefront, but the theory predicts an infinite value of the breakdown time nevertheless (again, see Section 3). However, we should note that the absence of an acceleration wave does not preclude the steepening of the profile *behind* the wavefront, i.e., for $x < t$.

In Figs. 1 and 2, the red and blue curves correspond to the LW and Euler equations, respectively, and the dashed curves denote the (properly rescaled) linear solution. In Fig. 1, the solid black lines were generated from Eq. (20) and denote the tangent line to the profile at the wavefront Σ as predicted by singular-surface theory. We performed simulations for several values of the Mach number. As expected, the LW system was found to be in close agreement with the Euler equations only for smaller values of ϵ.

From Fig. 1 it is clear that even for a Mach number as large as $\epsilon = 0.265$ (given that $\epsilon \ll 1$ by the finite-amplitude assumption), the LW system is in good agreement with the Euler equations, at least for small values of t. Moreover, the slope at the wavefront, as numerically determined, was found to be in excellent agreement with the predictions of singular surface theory. In addition, the conservative LW formulation presented here yields a profile that is, in essence, indistinguishable from the one generated in [7], which is represented by the black dots in Fig. 1 for $t = 0.95$.

As Fig. 1 clearly shows, the LW system predicts a faster rate of steepening of the profile than the Euler equations. This is an important finding that we attribute to what can be loosely called "saturation of the nonlinearity." In other words, under the finite amplitude approximation, the nonlinear terms are not bounded, while under the framework of the exact theory (Euler equations), the nonlinearity is a bounded function of the dependent variable u. Thus, for larger u the LW profile exhibits a much faster steepening than the corresponding Euler profile, since the former is subject to saturation of the nonlinear term.

Fig. 2 presents the numerical solution for the second choice of BC, for which finite-time blow-up does not occur at the wavefront. The conventions for the curves are the same as in Fig. 1. Here, two different Mach numbers are considered. The first, $\epsilon = 0.1$ (shown in the left panel of frames in Fig. 2), is small enough so that the predictions of the two models are expected to be very close; and indeed they are up to $t = 2.00$, which is a relatively large time. Moreover, it is clear that there is no shock at the wavefront; however, the profile steepens continuously in the region behind Σ. Once again, the profile governed by the LW system tends to steepen faster than the profile governed by the Euler system. For $t = 1.00$ and $\epsilon = 0.265$, it appears that the LW profile has already developed a shock behind the wavefront. Similarly, the Euler profile appears to develop a shock, but at a later time. Also, note that in both cases, there is no shock in the vicinity of the wavefront. Lastly, it should be noted that the simple, explicit finite-difference scheme given in [7] was found to be ill-suited for this (second) choice of BC.

7. Conclusions

We have examined the propagation of acoustic signals produced by two different sinusoidal BCs, as modeled by the Euler system of equations and by the LW equation, the latter being

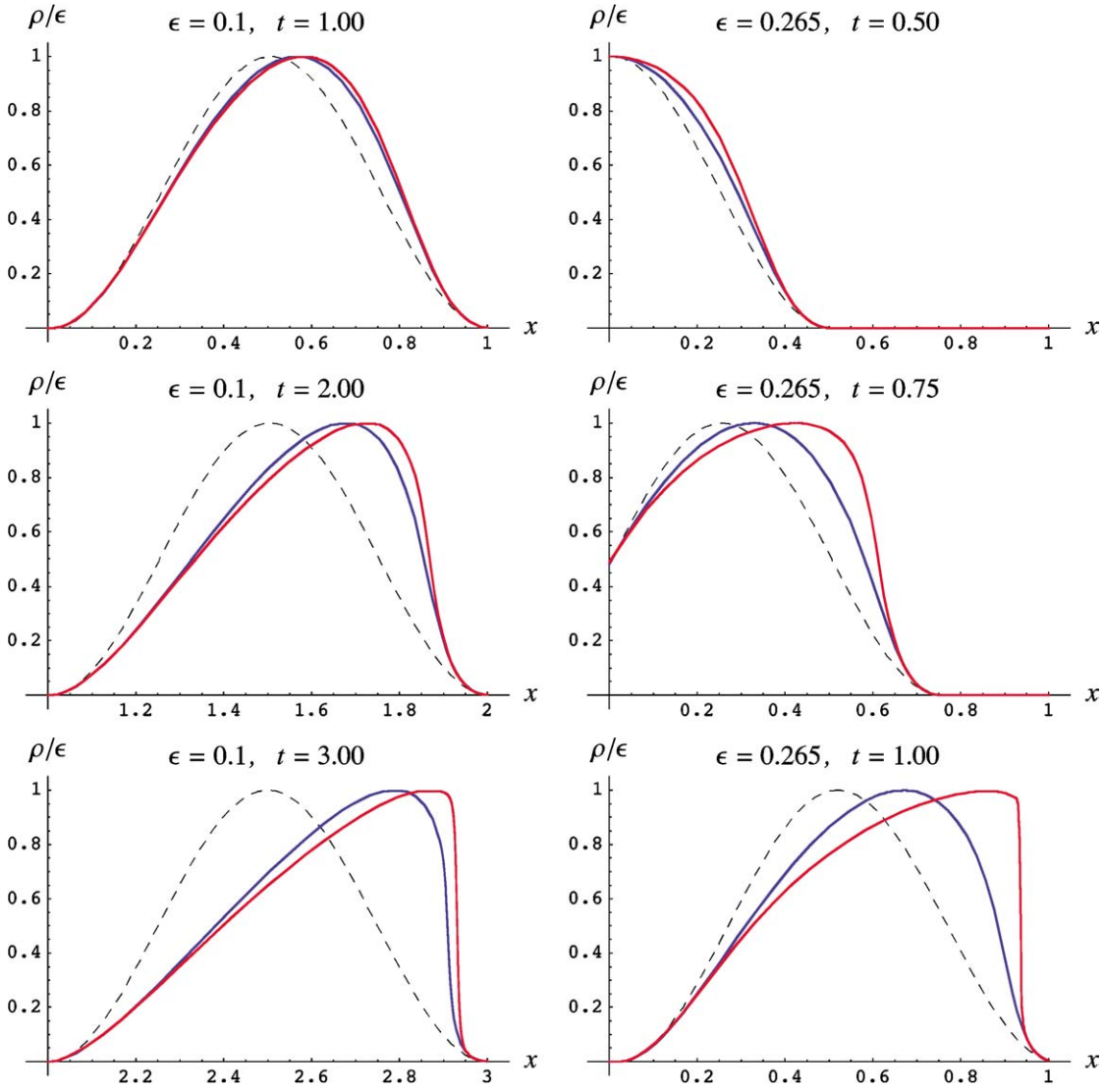

Fig. 2. Three snapshots in time of the scaled dimensionless acoustic density, ρ/ϵ, vs. x for $f(t) = \epsilon \sin^2(\pi t)$ and two different values of ϵ.

a weakly nonlinear approximation of the former in which the linear-impedance assumption is also used. Specifically, we employed a Godunov-type shock-capturing scheme to compute the numerical solutions of the former and latter for relatively large times. Additionally, we reformulated the LW equation as a conservation law using a new set of dependent variables and, to support our numerical work, we also presented an acceleration wave analysis of the Euler equations.

For the compressive BC (see Fig. 1), our numerical scheme did a very good job of capturing the "shocking-up" of the profiles as the time of blow-up approached. In fact, the numerically predicted time of blow-up was in excellent agreement with that of the theory (see Section 3) for both systems. Of particular interest was the finding that the rate of steepening predicted by the LW system is much greater than that predicted by the Euler equations. In contrast, for the second BC considered (see Fig. 2), the theory predicts that there is no acceleration wave, and that the breakdown time is infinite. However, our simulations suggest that the profile develops a discontinuity in the region *behind* the wavefront (i.e., $x < t$) in finite time. Nonetheless, this does not contradict our theoretical prediction of an infinite breakdown time for this case, since the results of Section 3 apply strictly *at* the wavefront. (Because the steepening of the profile behind the wavefront is clearly different from that which contributes to acceleration wave blow-up in finite time, and thus is atypical of what can be found in the literature, we feel that the former warrants further study.) Lastly, an important finding of our simulations for this (second) BC is that, just as it did for the first BC, the LW equation predicts much steeper profiles and a more rapid rate of shocking-up than do the Euler equations, limiting its applicability to small values of t and ϵ. We explained the faster rate of steepening as a saturation effect.

Acknowledgements

The first two authors were supported by ONR/NRL funding (PE 061153N). All figures appearing in this Letter were generated using the software package MATHEMATICA (Version 5.2).

References

[1] P.J. Chen, in: S. Flügge, C. Truesdell (Eds.), Handbuch der Physik, vol. VIa/3, Springer, Berlin, 1973, pp. 303–402.
[2] B.D. Coleman, M.E. Gurtin, Phys. Fluids 10 (1967) 1454.
[3] B. Straughan, Ann. Mat. Pura Appl. 126 (1980) 187.
[4] G. Saccomandi, Int. J. Non-Linear Mech. 29 (1994) 809.
[5] H. Lin, A.J. Szeri, J. Fluid Mech. 431 (2001) 161.
[6] R. Quintanilla, B. Straughan, Proc. R. Soc. London A 460 (2004) 1169.
[7] P.M. Jordan, C.I. Christov, J. Sound Vib. 281 (2005) 1207.
[8] P.M. Jordan, A. Puri, Phys. Lett. A 341 (2005) 427.
[9] P.M. Jordan, Proc. R. Soc. London A 461 (2005) 2749.
[10] E.R. Toro, Riemann Solvers and Numerical Methods for Fluid Dynamics, Springer, Berlin, 1999.
[11] S.K. Godunov, Mat. Sb. 47 (1959) 271 (in Russian).
[12] B. van Leer, J. Comput. Phys. 32 (1979) 101.
[13] R.J. LeVeque, Finite Volume Methods for Hyperbolic Problems, Cambridge Univ. Press, New York, 2002, pp. 203–253.
[14] P.A. Thompson, Compressible-Fluid Dynamics, McGraw–Hill, New York, 1972.
[15] K. Naugolnykh, L. Ostrovsky, Nonlinear Wave Processes in Acoustics, Cambridge Univ. Press, New York, 1998, Chapter 1.
[16] W. Chester, Proc. R. Soc. London A 434 (1991) 459.
[17] R.L. Bisplinghoff, H. Ashley, R.L. Halfman, Aeroelasticity, Addison–Wesley, Cambridge, MA, 1955.
[18] M.F. Hamilton, C.L. Morfey, in: M.F. Hamilton, D.T. Blackstock (Eds.), Nonlinear Acoustics, Academic Press, New York, 1997, pp. 41–63.
[19] H. Ockendon, J.R. Ockendon, Meccanica 36 (2001) 297.
[20] A. Harten, P.D. Lax, B. van Leer, SIAM Rev. 25 (1983) 35.